Nanoscale

RSC Publishing

PAPER

View Article Online
View Journal | View Issue

Cite this: *Nanoscale*, 2013, **5**, 7271

Nonlinear optical properties of boron doped single-walled carbon nanotubes

Benoy Anand,[a] Ramakrishna Podila,[bc] Paola Ayala,[d] Luciana Oliveira,[b] Reji Philip,[e] S. Siva Sankara Sai,[a] Anvar A. Zakhidov[f] and Apparao M. Rao*[bg]

Received 10th April 2013
Accepted 28th May 2013

DOI: 10.1039/c3nr01803b

www.rsc.org/nanoscale

Single-walled carbon nanotubes (SWCNTs) exhibit excellent nonlinear optical (NLO) properties due to the delocalized π electron states present along their tube axis. Using the open aperture *Z*-scan method in tandem with X-ray photoelectron spectroscopy (XPS) and Raman spectroscopy, we demonstrate the simultaneous tailoring of both electronic and NLO properties of SWCNTs, from ultrafast (femtosecond) to relatively slow (nanosecond) timescales, by doping with a single substituent, *viz.*, boron. SWCNTs were doped *via* a wet chemical method using B_2O_3, and the boron content and bonding configurations were identified using XPS. While in the ns excitation regime, the nonlinear absorption was found to increase with increasing boron concentration in the SWCNTs (due to the increasing disorder and enhanced metallicity of the SWCNTs), the saturation intensity in the fs excitation regime decreased. We attribute this counter-intuitive behavior to excited state absorption on ns timescales, and saturable absorption combined with weak two-photon transitions on fs timescales between van Hove singularities.

Introduction

A substitutionally doped carbon nanotube[1] is an ideal system in which novel fundamental properties have been realized, *e.g.*, renormalization of the electron–phonon energies at the dopant site,[2] onset of superconductivity in boron (B)-doped single-walled carbon nanotube (SWCNT) bundles,[3–5] and permanent n- or p-type characteristics in nitrogen- or B-doped carbon nanotubes.[6–8] Detailed synthesis, microscopic and spectroscopic studies found a strong correlation between the local bonding environment of the dopant and the influence of dopant states present near the Fermi level on the electronic and optical properties of doped carbon nanotubes.[8–10] Of interest to this study is the influence of dopant states on the nonlinear optical (NLO) properties of SWCNT bundles, which result from the delocalized π electron cloud present along the tube axis. The high third-order nonlinear polarizability ($\chi^{(3)} \sim 10^{-7}$ to 10^{-10} esu) and subpicosecond carrier dynamics of SWCNTs are well suited for ultrafast optical switches.[11] SWCNTs are also well-studied for mode locking[12] and optical limiting (OL) applications.[13]

Dopant-induced changes in the electronic band structure of SWCNTs are expected to influence their NLO properties. Indeed, Xie *et al.* predicted an enhancement in the second order hyper-polarizability in B-doped zigzag nanotubes, due to the dopant induced changes in the π electron cloud.[14] In this regard, a comprehensive experimental study on B-doped SWCNTs is pertinent to delineate the dopant effects on the NLO properties. Furthermore, NLO studies are of great assistance in pinpointing the dopant window where the electronic and optical properties are optimized for a particular application. Here, we present a systematic study describing the effects of substitutional B doping on the NLO properties of SWCNTs by correlating open aperture Z-scan measurements (carried out in both nanosecond (ns) and femtosecond (fs) excitation regimes) with XPS and Raman spectroscopy. We find that both the limiting and the saturation behaviors of B-doped SWCNTs can be tuned *via* B-induced changes in the disorder and metallicity of SWCNTs.

Experimental methods

High purity SWCNTs were obtained from Nanomaterial Store (Product no.: SN2102) and refluxed in a H_2O_2–HCl mixture for 72 hours to induce defects in their walls. Next, the refluxed SWCNTs were vacuum filtered using a 0.45 μm nylon membrane and washed thrice with boiling deionized water and dispersed into ethanol suspensions containing B_2O_3 powder with 0.04 (sample ID: S1), 0.08 (S2), and 0.32 (S3) M concentrations (Table 1). Following a 1 h bath sonication and evaporation of the ethanol, the B_2O_3–SWCNT mixtures were annealed

[a]*Department of Physics, Sri Sathya Sai Institute of Higher Learning, Prashanti Nilayam, Andhra Pradesh, 515134, India*
[b]*Department of Physics and Astronomy, Clemson University, Clemson, SC, 29634, USA*
[c]*Brody School of Medicine, East Carolina University, Greenville, NC, 27834, USA*
[d]*Faculty of Physics, University of Vienna, Strudlhofgasse 4, A-1090, Vienna, Austria*
[e]*Light and Matter Physics Group, Raman Research Institute, Bangalore, 560080, India*
[f]*NanoTech Institute, University of Texas at Dallas, Richardson, TX 75083, USA*
[g]*Center for Optical Materials Science and Technology, Clemson University, Clemson, SC, 29634, USA. E-mail: arao@clemson.edu*

Table 1 The dopant content of three B-doped SWCNTs used in this study. The second column shows the nominal concentration of B_2O_3 used in the synthesis procedure for preparing samples S1, S2, and S3. The third column shows the percentage of B in substitutional configuration as determined from XPS

Sample ID	Nominal B_2O_3 concentration	Substitutional B content
S1	0.04 M	0.19%
S2	0.08 M	0.22%
S3	0.32 M	0.42%

at 180 °C in a 100 : 10 sccm Ar : H_2 gas flow for 2 h. Finally, all the samples were annealed in flowing Ar at 1000 °C for 30 min. Micro-Raman spectra of all samples were collected using a Dilor XY triple grating monochromator (100× objective) with 514.5 nm excitation from an Ar ion laser, and the XPS studies were carried out using a Phi spectrometer equipped with a monochromatic Al K_α source (1486.6 eV) with an overall resolution of 0.5 eV.

For the NLO measurements we employed the open aperture Z-scan method in the nanosecond (5 ns) and femtosecond (100 fs) excitation regimes, at 532 nm and 800 nm wavelengths, respectively. In this technique the laser pulses are focused onto a sample using a converging lens and the sample is translated from $-z$ to $+z$, where $z = 0$ represents the focal point. The nonlinear absorption (NLA) coefficient is calculated from the intensity dependent transmittance (T), which is measured as a function of z. We have detailed the open aperture Z-scan methodology employed in this study, elsewhere.[15] Samples S1, S2 and S3 were dispersed in dimethylformamide (DMF) to obtain a linear transmittance of 70%. The NLO measurements were performed on these dispersions in a 1 mm thick quartz cuvette. The pulse repetition rates were 0.25 and 10 Hz for the ns and fs excitations, respectively. From knife edge measurements, the beam waist at focus was calculated to be ~20 μm for the ns pulses and ~16 μm for the fs pulses.

Results and discussion

XPS studies

The C1s photoemission spectrum for pristine SWCNTs (which has been thoroughly investigated elsewhere[16]) shown in Fig. 1a exhibited a binding energy peak at ~284.45 eV. It is well known that the position of the C1s peak varies with B- or N-doping. Here, we found that the C1s peak was downshifted by ~0.15 eV in B-doped SWCNTs, in agreement with our previous results on laser ablated B-doped SWCNTs.[17] Furthermore, we observed that the C1s FWHM peak width in all the samples (S1, S2, and S3) is ~0.6 eV, similar to the laser ablated SWCNTs.

As shown in Fig. 1b–d, the B1s core signal may be deconvoluted into two peaks at 191.5 and 192.8 eV, which correspond to the presence of substitutional B in the SWCNT lattice and B_2O_3 respectively.[18] The latter peak (~192.8 eV) most likely is due to the residual B_2O_3 left in the samples during the synthesis procedure. The substitutional B-doping contents (see Table 1) for our samples were determined from the respective cross-sections of the C and B peaks and the areas under the C1s and B1s peaks.[18] As expected, we observed that the net substitutional B content increased with increasing nominal concentration of B_2O_3 in the synthesis.

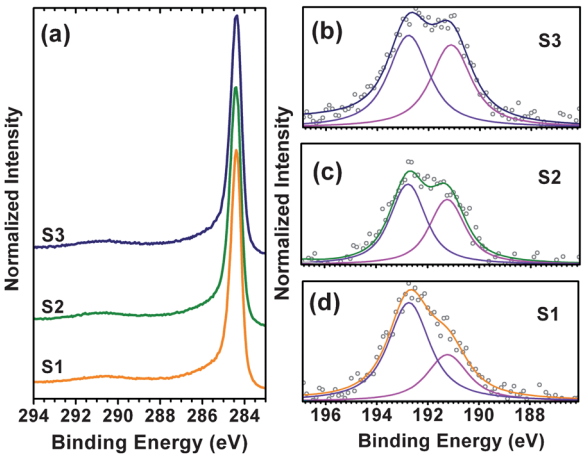

Fig. 1 The C1s (panel a) and the B1s lines (panels b–d) for the three B-doped samples used in this study.

Raman and NLO studies

Fig. 2a shows the representative Raman spectra for pristine and B-doped SWCNT bundles, obtained using 514.5 nm excitation. The diameter of the SWCNTs can be calculated using the well-known relation between the radial breathing mode frequency ω_{RBM} and the SWCNT diameter d in nm:

$$\omega_{RBM} = \frac{223.5\ \text{cm}^{-1}}{d} + 12.5\ \text{cm}^{-1}. \quad (1)$$

From the position of the RBM frequencies for pristine SWCNTs (140–240 cm^{-1}), their diameters are inferred to be in the range from 1.0 to 1.7 nm. The downshift in the RBM frequencies for the doped SWCNTs to 130–190 cm^{-1} is attributed to (i) the change in population distribution of SWCNTs during the acid treatment, and (ii) the change in the relative intensities of the RBMs due to doping. The energy gaps between the van Hove singularities (vHs) for the semiconducting (E_{ii}) and metallic (M_{ii}) SWCNTs can be obtained using the zone-folding method and are pictorially depicted using the well-known Kataura plot (Fig. 2b). In the Kataura plot, the solid vertical lines mark the dominant tube diameters as deduced from the RBM spectra of pristine and B-doped SWCNTs. Clearly, the SWCNTs in our samples predominantly couple to 532 nm (800 nm) *via* E_{33} and E_{44} (E_{22} and M_{11}).

As shown in Fig. 3a, our detailed open aperture Z-scan experiments on both pristine and B-doped SWCNTs revealed OL in the ns excitation regime (532 nm, 2.33 eV) and saturable absorption (SA) in the fs excitation regime (800 nm, 1.55 eV). Numerically, the nonlinear transmission equation pertaining to two-photon absorption (2PA) best-fitted the measured data, with an r^2 of 0.992 and 0.977 for pristine nanotubes and S3

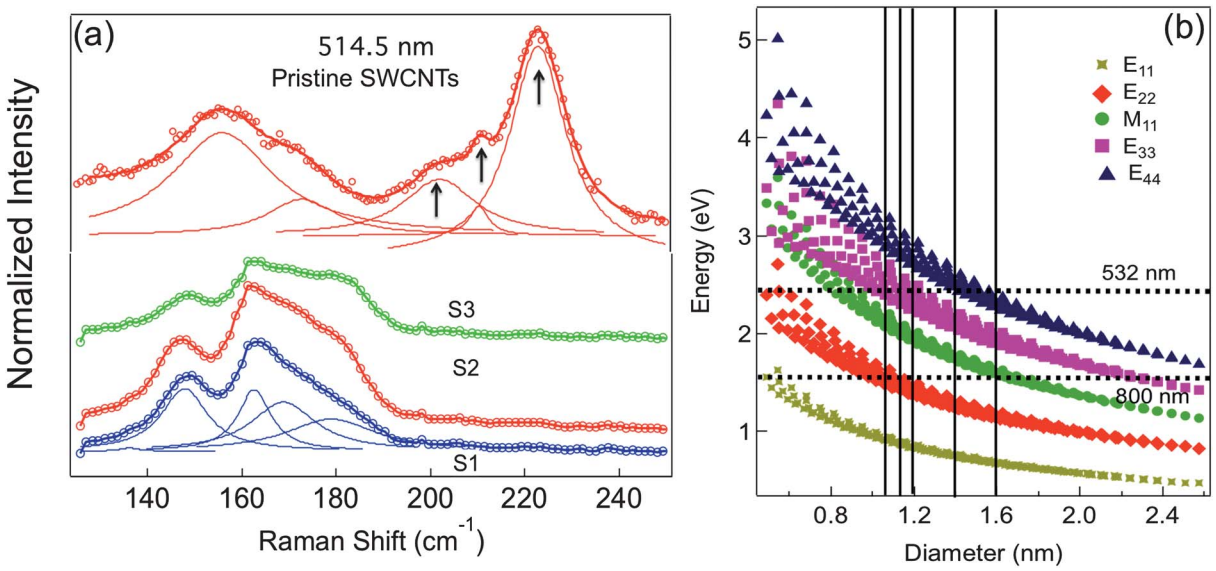

Fig. 2 (a) A representative Raman spectrum showing the radial breathing modes of pristine and B-doped SWCNT bundles. The disappearance of higher frequency modes (shown by black arrows; corresponding to smaller diameter tubes) is possibly due to the acid treatment of SWCNTs. The Kataura plot in (b) shows that the SWCNTs, dominant diameters of which are indicated by the solid vertical lines, couple to the 532 nm (800 nm) excitation *via* E_{33} and E_{44} (E_{22} and M_{11}).

respectively, in the case of ns excitation (see Fig. 3a). The pulse propagation equation for a 2PA process, $dI/dz' = \alpha_0 I - \beta I^2$, can be solved for the sample transmittance as

$$T = \left((1-R)^2 \exp(-\alpha_o L)\Big/\sqrt{\pi} q_o\right) \int_{-\infty}^{+\infty} \ln\left[1 + q_o^2 \exp(-t^2)\right] dt, \quad (2)$$

where L and R are the sample length and surface reflectivity respectively,[19] I is the incident beam intensity, α_o is the unsaturated linear absorption coefficient, and z' is the propagation distance within the sample. In eqn (2), q_o is given by $\beta(1-R)I_o L_{eff}$, where β is the two-photon absorption coefficient, I_o is the on-axis peak intensity, and the effective length L_{eff} is given by $(1-\exp(-\alpha_o L))/\alpha_o$. On the other hand, both pristine and B-doped SWCNTs exhibit SA behavior with the fs excitation (Fig. 3a). However, a best fit is obtained (with an r^2 of 0.994 and 0.978 for pristine nanotubes and S3 respectively) when a weak 2PA process is included in the model in addition to absorption saturation (SA + 2PA). The nonlinear transmittance for a SA + 2PA process can be obtained by numerically solving the pulse propagation equation

$$\frac{dI}{dz'} = -\frac{\alpha_o I}{1 + I/I_s} - \beta I^2, \quad (3)$$

where I_s is the saturation intensity, given by $I_s = h\upsilon/2\sigma\tau$. Here h is Planck's constant, υ is the photon frequency, σ is the absorption cross-section for the transition and τ is the excited state life time.[19] Details of these processes and the fitting procedure are described in ref. 20. It is important to note that a numerical fit to a given set of Z-scan data using the 2PA transmission equation does not necessarily indicate the exclusive occurrence of two-photon absorption; rather, it may as well correspond to an excited state absorption (ESA) process.[21] As a macroscopic parameter that depends on the concentration of two-photon absorbing molecules β can be expressed as $\beta = \sigma\Delta N/h\upsilon$ where σ is the 2PA cross-section of the material, $h\upsilon$ is the photon energy of the laser beam and $\Delta N = N_0 - N_1$ is the population density difference between the ground state (N_0) and the two-photon excited state (N_1). 2PA is a weak process as it usually involves *virtual* intermediate states, and the population depletion of the ground state is negligible ($N_1 \sim 0$ *or* $\Delta N \sim N_0$) for a large range of input intensities. Therefore, in practice β does not vary with input intensity. On the other hand ESA is a strong process due to the involvement of *real* intermediate states, and ground state depletion is considerable, making β a function of input intensity. With increasing intensity, depletion of the ground state population increases, leading to a reduction of β values.[22] We discuss this point in greater detail below.

The NLA in SWCNTs is well-understood in terms of the interband transitions between their vHs.[23] The absorption mechanisms are quite different in metallic and semiconducting SWCNTs (m-SWCNTs and s-SWCNTs). While excitons are the primary type of photo-excitations in s-SWCNTs, free carrier absorption dominates the NLA in m-SWCNTs.[24] From the Kataura plot (Fig. 2b) it is easy to see that the ns excitation at 532 nm (2.33 eV) couples predominantly with the E_{33} and E_{44} of s-SWCNTs. The ESA occurring from these states to higher lying levels (see Fig. 4a) will result in the OL action. The reduction of β with on-axis peak intensity shown in Fig. 5a indicates ESA during ns excitation. On the other hand, SA observed with ultrafast pulses at 800 nm arises from m-SWCNTs, as the incident photon energy is resonant with M_{11} (see Fig. 4b).[25] Here, a high intensity excitation at 800 nm leads to a large temporally varying population of carriers in the conduction band. Further absorption of photons within the pulse duration is reduced due to Pauli blocking, giving rise to the increased transmittance seen in Fig. 3a. The weak 2PA component ($\sim 10^{-16}$ m W^{-1})

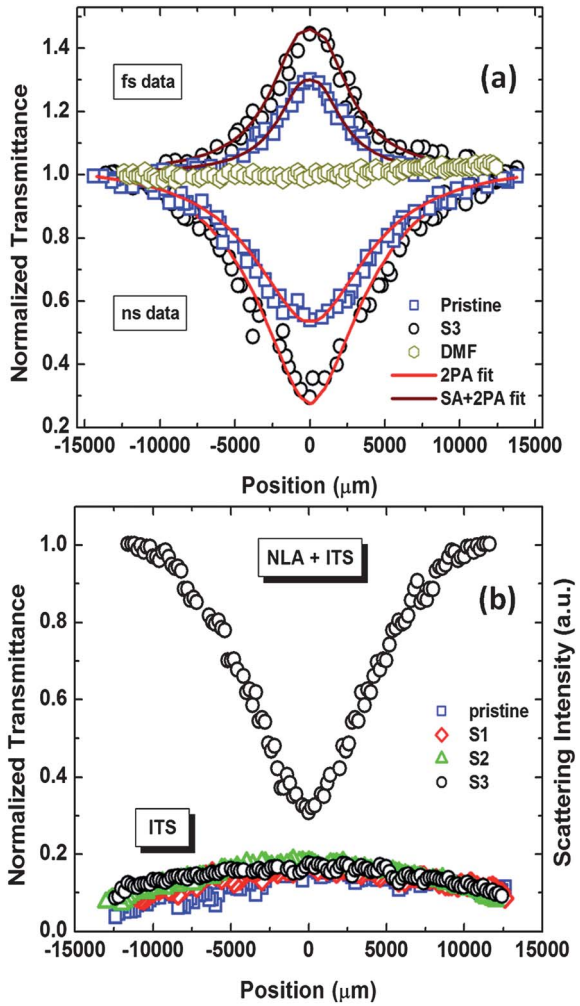

Fig. 3 (a) The open aperture Z-scan curves obtained for pristine SWCNTs and S3 with 5 ns pulses at 532 nm (I_0 = 5.7 GW cm^{-2}) and 100 fs pulses at 800 nm (I_0 = 37.3 TW cm^{-2}). The solid lines represent the fits to the experimental data as described in the text. Both limiting depth and saturation height increase with B doping. The flat ns Z-scan curve obtained for DMF suggests that the solvent nonlinearity is too weak to measure. (b) The relative strengths of NLA and ITS in the ns excitation regime (I_0 = 5.7 GW cm^{-2}).

present in the fs excitation regime (in addition to strong SA) arises from 2PA as well as ESA occurring in both m-SWCNTs and s-SWCNTs with the ESA being weak for the fs excitation relative to the ns excitation. As evident from Fig. 2b, the 800 nm excitation couples with E_{22}. However, ultrafast pump–probe studies done by Korovyanko *et al.* revealed that 800 nm pulses can excite E_{11} as well, even though the photons are not in resonance with this level.[24] ESA occurring from the corresponding excited states also contributes to the weak 2PA component. Thus from a device point of view, SWCNTs possess a unique advantage: depending on the excitation pulse-width and wavelength, they can potentially be used for laser safety applications (OL behavior) or pulse shaping, shortening and optical switching (SA behavior). Fig. 3b shows the scattering signal from the both pristine and B-doped samples, which will be discussed in detail in the last section.

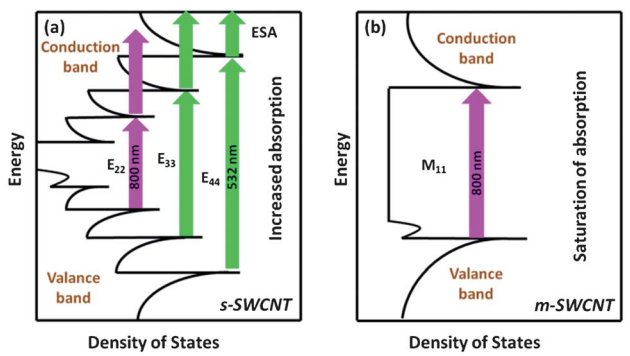

Fig. 4 A schematic depicting the major optical transitions between vHs that lead to NLA in B-doped (a) semiconducting and (b) metallic SWCNTs.

Effects of doping

In the ns excitation domain NLA increases with B doping, which is evident from the corresponding increase in β seen in Fig. 5a. The increase of metallic character with doping underlies this direct correlation between doping levels and β. Previous electrical transport[26] and scanning tunneling spectroscopy[9] studies have shown enhanced conductivity in B-doped nanotubes, which confirmed their metallic character.[27] The lowering of the Fermi level and formation of an acceptor state in the band gap due to B doping (see Fig. 4) explain the transformation of semiconducting tubes into metallic ones. The large number of free carriers produced in the metallic nanotubes at high incident intensities could then enhance NLA through strong free carrier absorption. The enhancement in β values can also be attributed to the shift in the RBM frequencies upon doping (see Fig. 2), which brings more electrons in the nanotubes into resonance with the incident photon.[28]

From our recent investigations in chemical vapor deposited polycrystalline graphene we have shown that a decrease in the in-plane crystallite size (or an increase in the defect density) leads to a reduction in the saturation intensity.[29] Similarly, for ultrafast excitation in our case, I_S values are found to decrease with doping concentration (Fig. 5b). From XPS studies, the concentration of substitutional B in the SWCNTs is found to vary in the order S3 > S2 > S1 (*cf.* Table 1). In the ns domain the variation of β with on-axis peak intensity I_o (as shown in Fig. 5a) suggests an ESA mechanism, where carrier excitation from the ground state to the excited state is mediated through a real intermediate state. It is evident from Fig. 5a that β values increase in the same order as the dopant percentage in the lattice (S3 > S2 > S1). These results agree with the fact that the B-dopants present in the SWCNT lattice act as defect centers and result in an increased NLA in the ns regime. The limiting threshold of S3 is measured to be 0.86 J cm^{-2} which is lower than previously reported bench mark materials like C_{60} (~2 J cm^{-2}),[30] carbon black (~2.2 J cm^{-2}),[30] MWCNTs (0.91 J cm^{-2})[30] and SWCNTs (1 J cm^{-2}).[13] Limiting in pristine nanotubes is not strong enough to measure the limiting threshold. Thus, the increase in NLA leads to the enhancement of OL efficiency, making B-doped SWCNTs better optical limiters than pristine SWCNTs. On the other hand, in the ultrafast regime the saturation depth increases (I_s decreases) with substitutional B content. This flexibility offers the possibility of tuning the

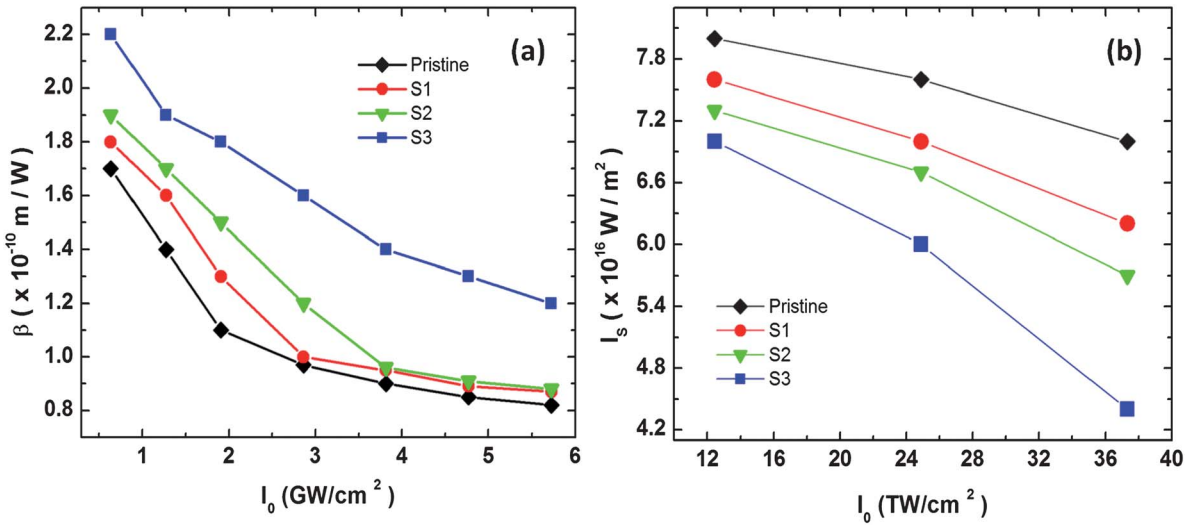

Fig. 5 (a) Variation of the nonlinear absorption coefficient β with on-axis peak intensity I_o in the ns excitation regime suggesting ESA when excited with the 532 nm photons. (b) Variation of the saturation intensity I_S with I_o in the fs excitation regime. The systematic reduction in I_S in B-doped SWCNTs is attributed to the increasing presence of defects in the SWCNTs.

ultrafast optical switching properties of SWCNTs by controlling the B content in the lattice. Thus, the OL and SA behaviors of doped nanotubes can be controlled simply by adjusting just one experimental parameter in the synthesis process, namely the initial concentration of B_2O_3. Therefore, substitutional B doping provides a very effective pathway for tailoring not only the electronic properties of SWCNTs, but also their nonlinear optical properties.

Effect of induced thermal scattering (ITS)

A number of previous NLO studies carried out on SWCNT suspensions have revealed that ITS is a major contributor to OL in the ns excitation regime (see for example the studies by Mishra *et al.*[13] and Vivien *et al.*[31]). Various mechanisms such as micro bubbles, micro plasma and refractive index variations have been proposed as possible causes. Since several ns are required for the formation of thermal scattering centers, their effect is usually not visible in the ultrafast excitation regime.[32] We have carried out scattering measurements in all samples used in this study by keeping an additional photodiode detector close to the sample at 45° to the beam axis in the usual Z-scan geometry, to determine the role of ITS in the observed NLO response. The scattered signals from both pristine and B-doped SWCNTs, measured by this photodiode at an input laser energy of 180 μJ, are shown in Fig. 3b. For comparison, the open aperture Z-scan curve obtained for S3 at the same incident energy is also shown in Fig. 3b. If the contribution from ITS was strong, it would have resulted in a sharp increase in the scattered signal intensity as the sample reached the $z = 0$ position.[33] Since the scattered signals are almost flat from $-z$ to $+z$, in Fig. 3b, we conclude that ITS is very weak, and attribute this effect to the stable dispersions used in this study. Thus, the heat generated locally upon laser irradiation is dissipated evenly to the surroundings and thereby reduces the formation of localized scattering centers. Also the low repetition rate (0.25 Hz) of the laser pulses mitigates the possibility of accumulative thermal effects during our measurements. These observations imply that the observed OL in Fig. 3a arises mainly from NLA occurring in the samples.

Conclusions

In summary, SWCNTs were doped with B *via* a wet chemical method using B_2O_3. High resolution XPS measurements provided a measure of B content in the samples and confirmed the presence of substitutionally doped B in the SWCNT's lattice. The RBM frequencies in tandem with the Kataura plot enabled us to identify specific electronic transitions across the vHs for the two excitations used in this study, 532 nm in the ns and 800 nm in the fs excitation regimes. NLO measurements using open aperture Z-scan revealed that pristine as well as B-doped SWCNTs exhibit OL due to ESA in the ns excitation regime, and saturation due to SA along with weak 2PA in the ultrafast fs excitation regime. The NLA was identified with transitions across the vHs in the SWCNTs' electronic density of states, and in both ns and fs excitation regimes, it was found to systematically vary with the B content in the nanotube lattice. Thus, from NLO measurements done in tandem with XPS measurements and Raman spectroscopy we find that substitutional B doping is effective in tailoring electronic as well as NLO properties of SWCNTs. Consequently, we have demonstrated the tunability of NLO properties by substitutional B doping (determined by just a single synthesis condition), providing an easy route to enhance the scope of several NLO applications employing SWCNTs such as optical limiting, pulse shortening and optical switching.

Acknowledgements

Authors from SSSIHL thank Sri Sathya Sai Baba, the founder Chancellor, for the support and lab facilities. B.A acknowledges UGC, India for the senior research fellowship. P.A. was

supported by a Marie Curie Intra European Fellowship within the 7th European Community Framework Program. The authors thank Dr S. Sivaramakrishnan (IBM, Banglore) for the valuable discussions and suggestions.

Notes and references

1 P. Ayala, R. Arenal, A. Loiseau, T. Pichler and A. Rubio, *Rev. Mod. Phys.*, 2010, **42**, 1843.
2 I. Maciel, N. Anderson, M. A. Pimenta, A. Hartschuh, H. Qian, M. Terrones, H. Terrones, J. Campos-Delgado, A. M. Rao, L. Novotny and A. Jorio, *Nat. Mater.*, 2008, **7**, 878.
3 N. Murata, J. Haruyama, J. Reppert, A. M. Rao, T. Koretsune, S. Saito, M. Matsudaira and Y. Yagi, *Phys. Rev. Lett.*, 2008, **101**, 027002.
4 J. Haruyama, M. Matsudaira, T. Shimizu, J. Nakamura, T. Eguchi, T. Nishio, Y. Hasegawa, H. Sano, Y. Iye, J. Reppert and A. M. Rao, *Superlattices Microstruct.*, 2009, **46**, 333.
5 J. Nakamura, M. Matsudaira, J. Haruyama, H. Sugiura, M. Tachibana, J. Reppert, A. M. Rao, T. Nishio, Y. Hasegawa, H. Sano and Y. Iye, *Appl. Phys. Lett.*, 2009, **95**, 142503.
6 G. Keskar, R. Rao, J. Luo, J. Hudson and A. M. Rao, *Chem. Phys. Lett.*, 2005, **412**, 269.
7 B. Sadanadan, T. Savage, J. Gaillard, S. Bhattacharya, T. Tritt, A. Cassell, Z. Pan, Z. L. Wang and A. M. Rao, *J. Nanosci. Nanotechnol.*, 2003, **3**, 99.
8 P. Ayala, R. Arenal, M. Rümmeli, A. Rubio and T. Pichler, *Carbon*, 2010, **48**, 575.
9 D. L. Carroll, Ph. Redlich, X. Blase, J.-C. Charlier, S. Curran, P. M. Ajayan, S. Roth and M. Rühle, *Phys. Rev. Lett.*, 1998, **81**, 2332.
10 L.-J. Li, M. Glerup, A. N. Khlobystov, J. G. Wiltshire, J.-L. Sauvajol, R. A. Taylor and R. J. Nicholas, *Carbon*, 2006, **44**, 2752.
11 Y. C. Chen, N. R. Raravikar, L. S. Schadler, P. M. Ajayan, Y. P. Zhao, T. M. Lu, G. C. Wang and X. C. Zhang, *Appl. Phys. Lett.*, 2002, **81**, 975.
12 Y. W. Song, S. Yamashita and S. Maruyama, *Appl. Phys. Lett.*, 2008, **81**, 021115.
13 S. R. Mishra, H. S. Rawat, S. C. Mehendale, K. C. Rustagi, A. K. Sood, R. Bandyopadhyay, A. Govindaraj and C. N. R. Rao, *Chem. Phys. Lett.*, 2000, **317**, 510.
14 R. H. Xie, *Chem. Phys. Lett.*, 1999, **310**, 379.
15 B. Anand, S. A. Ntim, V. S. Muthukumar, S. S. S. Sai, R. Philip and S. Mitra, *Carbon*, 2011, **49**, 4767.
16 P. Ayala, Y. Miyata, K. D. Blauwe, H. Shiozawa, R. Silva, R. Follath, H. Kataura, C. Kramberger and T. Pichler, *Phys. Rev. B: Condens. Matter Mater. Phys.*, 2009, **80**, 205427.
17 P. Ayala, W. Plank, A. Grüneis, E. I. Kauppinen, M. Rümmeli, H. Kuzmany and T. Pichler, *J. Mater. Chem.*, 2008, **18**, 5676.
18 P. Ayala, J. Reppert, M. Grobosch, M. Knupfer, T. Pichler and A. M. Rao, *Appl. Phys. Lett.*, 2010, **96**, 183110.
19 R. L. Sutherland, *Handbook of Nonlinear Optics*, Marcel Dekker Inc., New York, 2nd edn, 2003, ch. 9, pp. 580–615.
20 V. S. Muthukumar, R. Podila, B. Anand, S. S. S. Sai, K. Venkataramaniah, R. Philip and A. M. Rao, in *Encyclopedia of Nanotechnology*, ed. B. Bhushan, Springer-Verlag, Heidelberg, 1st edn, 2013, pp. 1895–1911.
21 M. Rumi and J. W. Perry, *Adv. Opt. Photonics*, 2010, **2**, 451.
22 R. Podila, B. Anand, J. P. West, R. Philip, S. S. S. Sai, J. He, M. Skove, S.-J. Hwu, S. Tewari and A. M. Rao, *Nanotechnology*, 2011, **22**, 095703.
23 Y. Sakakibara, S. Tatsuurai, H. Kataura, M. Tokumoto and Y. Achiba, *Jpn. J. Appl. Phys., Part 1*, 2003, **42**, 494.
24 O. J. Korovyanko, C. -X. Sheng, Z. V. Vardeny, A. B. Dalton and R. H. Baughman, *Phys. Rev. Lett.*, 2004, **92**, 017403.
25 N. Kamaraju, S. Kumar, B. Karthikeyan, A. Moravsky, R. O. Loutfy and A. K. Sood, *Appl. Phys. Lett.*, 2008, **93**, 091903.
26 B. Wei, R. Spolenak, P. Kohler-Redlich, M. Rühle and E. Arzt, *Appl. Phys. Lett.*, 1999, **74**, 3149.
27 J. Vavro, J. M. Kikkawa and J. E. Fischer, *Phys. Rev. B: Condens. Matter Mater. Phys.*, 2005, **71**, 155410.
28 K. McGuire, N. Gothard, P. L. Gai, M. S. Dresselhaus, G. Sumanasekera and A. M. Rao, *Carbon*, 2005, **43**, 219.
29 R. Podila, B. Anand, J. T. Spear, P. Puneet, R. Philip, S. S. S. Sai and A. M. Rao, *Nanoscale*, 2012, **4**, 1770.
30 P. Chen, X. Wu, X. Sun, J. Lin, W. Ji and K. L. Tan, *Phys. Rev. Lett.*, 1999, **82**, 2548.
31 L. Vivien, P. Lancon, D. Riehl, F. Hache and E. Anglaret, *Carbon*, 2002, **40**, 1789.
32 N. Kamaraju, S. Kumar, A. K. Sood, S. Guha, S. Krishnamurthy and C. N. R. Rao, *Appl. Phys. Lett.*, 2007, **91**, 251103.
33 S. Sivaramakrishnan, V. S. Muthukumar, S. S. S. Sai, K. Venkataramaniah, J. Reppert, A. M. Rao, M. Anija, R. Philip and N. Kuthirummal, *Appl. Phys. Lett.*, 2007, **91**, 093104.

